Chaos, Solitons and Fractals 104 (2017) 6–17

Contents lists available at ScienceDirect

Chaos, Solitons and Fractals

Nonlinear Science, and Nonequilibrium and Complex Phenomena

journal homepage: www.elsevier.com/locate/chaos

# Watermarking based on discrete wavelet transform and $q$-deformed chaotic map

S. Behnia[a,*], M. Yahyavi[b], R. Habibpourbisafar[a]

[a] Department of Physics, Urmia University of Technology, Urmia, Iran
[b] Department of Physics, Bilkent University, TR-06800 Bilkent, Ankara, Turkey

ARTICLE INFO

*Article history:*
Received 28 March 2017
Revised 25 July 2017
Accepted 26 July 2017

*Keywords:*
$q$-deformed chaotic map
Pseudo random sequence
Ergodicity
Digital image watermarking
Key space
Security,

ABSTRACT

Hierarchy of one-dimensional ergodic chaotic maps with Tsallis type of $q$-deformation are studied. We find that in the chaotic region, these maps with $q$-deformation are ergodic as the Birkhoff ergodic theorem predicts. $q$-deformed maps are defined as ratios of polynomials of degree $N$. Hence, by using the Stieltjes transform approach (STA), invariant measure is proposed. In addition, considering Sinai-Ruelle-Bowen (SRB) measure, Kolmogorov-Sinai (KS) entropy for $q$-deformed maps is calculated analytically. The new $q$-deformed scheme have ability to keep previous significant properties such as ergodicity, sensitivity to initial condition. By adding $q$-parameter to the hierarchy in order increase the randomness and one-way computation, we present a new scheme for watermarking. The introduced algorithm tries to improve the problem of failure of encryption such as small key space, encryption speed and level of security. To illustrate the effectiveness of the proposed scheme, some security analyses are presented. By considering the obtained results, it can be concluded that, this scheme have a high potential to be adopted for watermarking. It can be concluded that, the proposed novel watermarking scheme for image authentication can be applied for practical applications.



## 1. Introduction

Digital watermarking technique is one of the popular research fields in signal processing, which can be used for multimedia protection [1]. The digital watermark should stick to the host data such that it provides a robust way of protecting digital multimedia information from illegal manipulation and duplication. The watermarking of multimedia information such as images [2,3], video [4,5] and audio [6] is already well developed. At present, many watermarking techniques from an aspect of preserving the watermark in the host data are categorized to three main groups: robust watermarking algorithms, fragile watermarking algorithms and semi-fragile watermarking algorithms [1,7,8]. On the basis of the information required during extraction algorithm, watermarking techniques can be classified into three categorizes: non-blind watermarking, semi-blind watermarking, and blind watermarking [8,9]. If the original host image is required to extract the embedded watermark, the technique is non-blind watermarking [10].

Digital watermarking methods can be broadly categorized as: transform domain watermarking, as in [11,12], and spatial domain watermarking such as in [13]. In most spatial domain techniques, watermark data is embedded in the least significant bit of the pixels in the host image [14]. Advantages of this method are their simplicity in embedding and extraction algorithm, improving the quality of watermarked image using Least Significant Bit (LSB), and increasing the speed of embedding and extraction process. Disadvantages of LSB method is weak against to common signal processing attacks on watermarked image [15]. Another method for watermarking is used transform domain to embedding and extracting the watermark. One of the advantages of this watermarking methods is the possibility to analyze and control their spectral properties and robustness against attacks. Taking more processing time for transform and inverse transform is disadvantage of this method. Transform domain watermarking schemes first apply transformation techniques, such as the discrete cosine transform (DCT) [16,17], discrete wavelet transform (DWT) [18,19], fractional Fourier transform (FrFT) [20,21] and singular value decomposition (SVD) [22,23] to an image. Watermark is then embedded by modifying the transform coefficients. The majority of watermarking schemes are using watermarks generated from pseudo random number sequences [15]. There is a large number of digi-

* Corresponding author. Tel.: +90 5534313007; fax: +90 312 266 4579.
*E-mail addresses:* s.behnia@sci.uut.ac.ir (S. Behnia), m.yahyavi@bilkent.edu.tr (M. Yahyavi).

http://dx.doi.org/10.1016/j.chaos.2017.07.020
0960-0779/

tal watermarking schemes, which the major drawback of them is lack of safety. For last couple of decades, chaotic functions such as coupled chaotic maps, skew tent map, Markov maps, Logistic map, Arnold map, and Bernoulli maps have been widely used to generate watermark sequences [14,15,24,38–40]. These types of watermark generation schemes require two values, the function seed and the initial value, in order to recreate the same watermark at a later stage. An advantage of watermarking based on chaotic maps is their robustness to low pass attacks. In order to enhance the security in watermarking process, it is desirable to use $q$-deformed chaotic maps.

Quantum group theory has greatly contributed by mathematicians and physicists [25]. The mathematical application of quantum groups theory comeback to the1840's when Heine found its relation to the $q$-hypergeometric functions ($q$-series). In fact, prominent mathematicians such as Fermat, Euler and Jacobi ventured into the $q$-functions much earlier. The $q$-deformed relations of Heisenberg algebra as a model for the noncommutative structure that arises from quantum group [26]. The expression $q$-derivation has also been used extensively in the case of the $q$-derivatives with the $q$-Lorentz generators which gives the $q$-deformation of Poincaré algebra [27]. Generally, there is no unique $q$-deformation for a function. Therefore, various $q$-deformations for the same function can be found in different physical and mathematical contexts. As of yet, significant strides have been made for studding of different types of $q$-deformations for the logistic map, which is the famous model of discrete dynamical system. For instance, the authors of Ref. [28] showed that the co-existence of attractors in $q$-logistic maps. Patidar et al. [29–31] compared that the dynamical behavior of the $q$-deformed Gaussian map. Recently, Shrimali et al. [32] demonstrated that the effect of delay on two forms of $q$-deformations of the logistic map. They also argued that chaotic behavior is suppressed in a certain region of delay and deformation parameter space. In this paper, the hierarchy of $q$-deformation maps has been presented based on the generalized Chebyshev polynomials type I and II. Compared with the well-known $q$-deformation chaotic maps, the proposed family of $q$-deformation chaotic maps have good properties such as co-existence of attractors, ergodicity, and semigroup property.

This paper mainly focuses on the application of the $q$-deformed maps in encryption schemes of watermark logos. More specifically it aims at proposing a secure watermarking scheme based on DWT and $q$-deformed chaotic maps. This algorithm tries to address the shortcoming of the previous watermarking processes such as small key space and limited speed. The $q$-deformed maps are employed to improve the security of a watermarked image. The $q$-series of the introduced dynamical system regarding the level of the security and the extra parameter can be used to apply many logos in watermarking process. Since $q$-deformed chaotic maps are sensitive to initial values, initial values of the $q$-deformed maps and their $q$-deformed parameters are exploited as secret keys in our algorithm. Experimental results and security analysis demonstrated that, the watermarked algorithm based on the $q$-deformed chaotic map is advantageous from the point of view of high level of security and large key space.

The rest of this paper is organized as follows. In Section 2, a brief description of basic deformations of one-dimensional chaotic maps is presented. In Section 3, it is shown how the degree of the chaoticity in the Tsallis type deformation system can be measured by KS-entropy. The watermarking scheme based on chaotic maps is proposed in Section 4. Also, the selected example and simulation results are discussed in Section 5. In Section 6, security of the chaotic encryption algorithm is explored. Section 7 summaries the paper. Two appendices are also provided, which contain all algebraic calculations and proofs.

## 2. The $q$-deformation of one-dimensional maps

The hierarchy of the $q$-deformed nonlinear maps can be defined as:

$$\begin{cases} \Psi_N(x_{n+1}, \alpha, q) = \Phi_N([x_n], \alpha) \\ [x] = \dfrac{x}{1+(1-q)(1-x)} \end{cases} \tag{1}$$

Here $q \in (-\infty\ -2]$ for $x$ in the interval [0, 1] and $x_n$ denotes the value of $x$ after $n$ iterations. In addition, when $q \to 1$ an hierarchy of $q$-deformed nonlinear maps reduces to the original maps. By considering the $\Phi_N^{(2)}(x, \alpha)$ families (See Appendix A), we have produced the following examples with the substitution $1 - q = \varepsilon$,

$$\Psi_2 = \frac{4\alpha^2(1+\varepsilon)x_n(1-x_n)}{(1+\varepsilon)^2 + x_n\left(4(\alpha^2-1) - 2\varepsilon^2 - 2\varepsilon\right) + x_n^2\left(4(-\alpha^2+1) + \varepsilon^2\right)} \tag{2}$$

$$\Psi_3 = \frac{\alpha^2 x_n(x_n(3\varepsilon+4) - 3(1+\varepsilon))^2}{\alpha^2 x_n(x_n(3\varepsilon+4) - 3(1+\varepsilon))^2 + ((1+\varepsilon)(1-x_n))(x_n(\varepsilon+4) - (\varepsilon+1))^2}$$

which under the limit $\varepsilon \to 0$, becomes the canonical maps of Eq. (A.2).

Fig. 1 gives the bifurcation diagram of the $\Psi_2(x_n, \alpha, \varepsilon)$ for $\varepsilon = 0,\ 4,\ -0.5$, and $-0.99$ with respect to the different values of $\alpha$. As it can be seen from Fig. 1(a), the system has regular behavior for parameter values smaller than the critical point $\alpha < \alpha_c$, where $\alpha_c$ denotes the critical parameter value for the onset of chaos ($\alpha_c = \frac{1}{2}$). As shown in this figure for $\alpha \in [0,\ 1/2]$, the fixed point $x = 0$ is stable in the map $\Psi_2(x_n, \alpha, \varepsilon)$ and bifurcates without period$-n-$tupling scenario to chaos. Fig. 1(b) shows the bifurcation diagram as a function of control parameter. Obviously, for fixed $q$-deformation $q = 4$, confirms chaos suppression via inverse tangent bifurcation. Chaos born by applying an negative value of $q$. Fig. 1(c) and (d), show that chaos cannot be suppressed in the negative value of deformation parameter and the stable period-1 motion becomes chaotic ($\alpha < \alpha_c$). By using the $q$-deformed version of the one-dimensional map, it is found that chaotification of the system is achieved. In this work, we also find that not only the system is very sensitive to initial conditions and the parameter $\alpha$ but also it's very sensitive to an $q$-deformation ($q$) parameter. It is an interesting phenomenon because generating chaos (also called anticontrol of chaos or chaotification) has grown up as a challenging and interesting research direction in recent years [33–36]. It can be observed that generally there are two separate regions in the deformation parameter space ($\varepsilon$; $\alpha$) which are corresponding to the stable and chaotic states. The stable state is a V-shaped region at the left-hand side and spread in the whole right of the control parameter (See Fig. 2). Also, we can show that by increasing the value of the parameter $\alpha$ the chaotic motion gets suppressed in the V-shaped region. Using mathematical methods, we may infer that the $q$-deformation of the chaotic one-dimensional map leads to the suppression of the chaotic region to an stable state (period-1). For odd values of $N$, these maps have only fixed point attractor $x = 0$ for $\alpha \in (\frac{1}{N}, N)$, again they bifurcate to a chaotic region at $\alpha \geq \frac{1}{N}$, and remain chaotic for $\alpha \in (0, \frac{1}{N})$, finally they bifurcate at $\alpha = N$ to have $x = 1$ as fixed point attractor for all $\alpha \in (\frac{1}{N}, \infty)$. It also shows that for the positive value of $q$-deformation, the narrow channel is formed between the nonlinear map function and the diagonal line from the fixed point attractor $x = 0$. The regular behavior or the laminar region corresponds to an evolution of the system in a narrow region or a channel in the phase space. Such regular behavior stems from the fact that the system maintains a "ghost" of laminar region. It is clear that, the fixed point $x = 1$ loses stability for negative $\varepsilon$ and the chaotic zone reduces from the fixed point $x = 1$ by decreasing the value of $\varepsilon$ until $-1$.

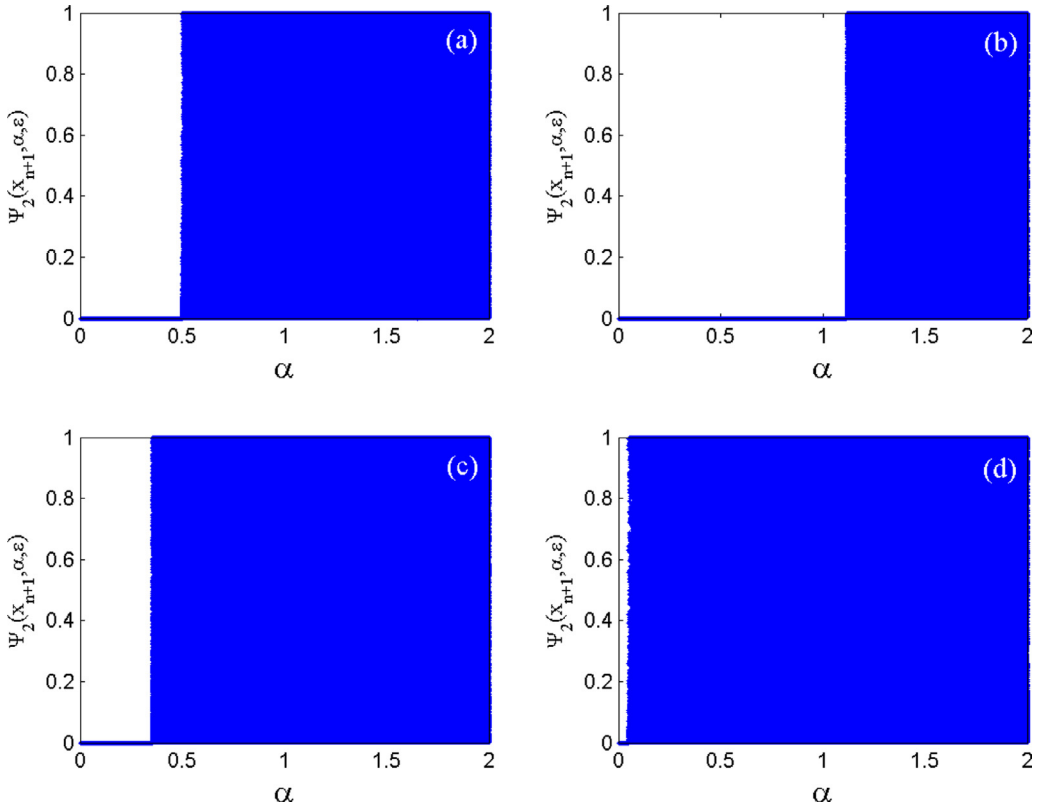


**Fig. 1.** Bifurcation diagram of the map $\Psi_2(x_{n+1},\alpha,\varepsilon)$ with respect to $\alpha$ for (a) $\varepsilon=0$, (b) $\varepsilon=4$, (c) $\varepsilon=-0.5$, (d) $\varepsilon=-0.99$.

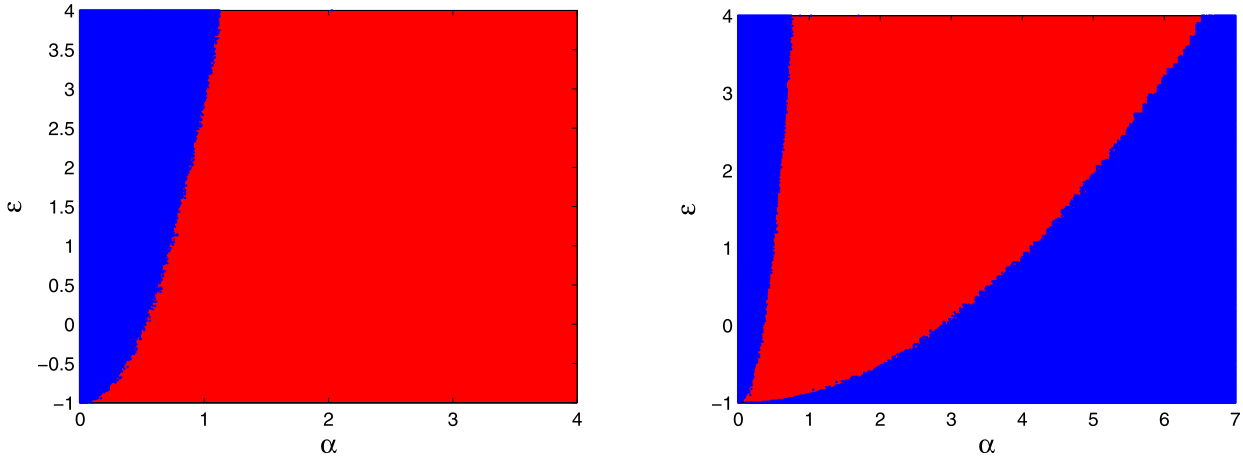


**Fig. 2.** The parameter space $(\alpha;\ \varepsilon)$ showing chaotic (red), stable state (blue) (a) $\Psi_2(x_{n+1},\alpha,\varepsilon)$ (b) $\Psi_3(x_{n+1},\alpha,\varepsilon)$. (For interpretation of the references to color in this figure legend, the reader is referred to the web version of this article.)

Parameter $\varepsilon$ ($q$-deformation parameter) lets us control the intermittent region and change the lengths of laminar phases. Also, we can show that middle V-shaped region by increasing the value of the parameter $\varepsilon$, the chaotic motion being increased. In what follows, we present the interesting properties of the above-described hierarchy of $q$-deformed nonlinear maps in detail Fig. 3.

## 3. Kolmogorov–Sinai entropy

Shannon entropy, regardless of what types of probabilities we use in it, cannot by itself identify chaos. A characteristic measure of chaos is the KS-entropy [37], which is related to Shannon's formula. If $P$ is a (measurable) partition, its entropy $H_\mu(P)$ with respect to the measure $\mu$ is defined as:

$$H_\mu(P) = -\sum_{A\epsilon P}\mu(A)\ln\mu(A), \tag{3}$$

for the introduced family, formula Eq. (3) should be rewritten as

$$h(\mu,\Psi_N(x,\alpha)) = \int dx\mu(x)\ln|\frac{d}{dx}\Psi_N(x,\alpha)|, \tag{4}$$

We obtain the following expression for the entropy of the map $\Psi_2(x_{n+1},\alpha)$:

$$h(\mu,\Psi_2(x,\alpha,\varepsilon)) = \int_0^1 \sum_{l=1}^{n}\lim_{x\to x_l}(x-x_l)G_\mu(x)\delta(x-x_l) \times \ln|\frac{d}{dx}\Psi_2(x,\alpha,\varepsilon)|dx$$

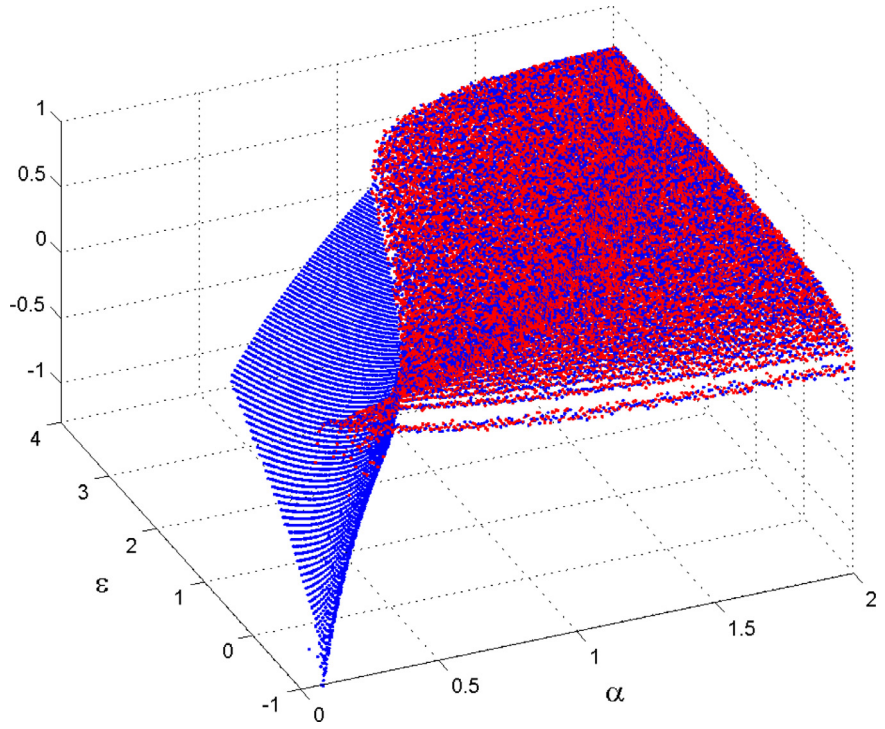


**Fig. 3.** Red dotted surface shows the variation of KS-entropy of $\Psi_2(x, \alpha, \varepsilon)$ in terms of the parameters $\alpha$ and $\varepsilon$, while blue dotted surface shows the variation of LCE of $\Psi_2(x, \alpha, \varepsilon)$ in terms of the parameters $\alpha$ and $\varepsilon$. (For interpretation of the references to color in this figure legend, the reader is referred to the web version of this article.)

by considering

$$\frac{d}{dx}\Psi_2 = \frac{4\alpha^2(1+\varepsilon)\left((\varepsilon+2)^2 - 4\alpha^2(1+\varepsilon)\right)}{\gamma-\chi} \times \left(\frac{\chi(1-\chi)}{(x-\chi)^2} + \frac{(\gamma-1)\gamma}{(x-\gamma)^2}\right) \tag{5}$$

then

$$h(\mu, \Psi_2(x,\alpha,\varepsilon)) = \int_0^1 \sum_{l=1}^{n} \lim_{x\to x_l}(x-x_l)G_\mu(x)\delta(x-x_l) \times (\ln|M(x-\gamma)^2 + N(x-\chi)^2| - 2ln|x-\chi| - 2ln|x-\gamma|)dx \tag{6}$$

where

$$\begin{cases} M(\gamma,\chi,\alpha) = \dfrac{4\alpha^2(1+\varepsilon)}{\gamma-\chi}(\chi-\chi^2) \\ N(\gamma,\chi,\alpha) = \dfrac{4\alpha^2(1+\varepsilon)}{\gamma-\chi}(\gamma^2-\gamma) \end{cases} \tag{7}$$

Due to avoid lengthening the present paper, we have considered only two terms of polynomial, as it was explained in calculation invariant manifold (SRB measure). It is clear that, by increasing the order of the summation in Eq. (6) the realistic form of KS entropy has been formed. We get the following expression for KS entropy:

$$h(\alpha,\epsilon,\Psi_2) = \ln\left(\sqrt{\frac{(M(K-\gamma)^2+N(K-\chi)^2)(M(K+\gamma)^2+N(K+\chi)^2)}{(K-\gamma)^2(K-\chi)^2(K+\gamma)^2(K+\chi)^2}}\right) \tag{8}$$

where

$$K = \sqrt{\frac{\left(4\alpha^2(1+\varepsilon)\left((\varepsilon+2)^2-4\alpha^2(1+\varepsilon)\right)\right)^2}{\chi^2-\gamma^2-\frac{\alpha^2}{1-\alpha^2}\left((\varepsilon+2)^2-4\alpha^2(1+\varepsilon)\right)^4\left(\frac{3\chi^2(1+\gamma)^2}{\gamma^2}+(1+\chi)(\gamma+4)\right)}}$$

KS entropy and Lyapunov characteristic exponents (LCE) are two related ways of measuring 'disorder' in an ergodic system. LCE is the characteristic exponent of the rate of the average magnification of the neighborhood of an arbitrary point $X_0$ and it is denoted by $\Lambda(x_0)$ which is written as:

$$\Lambda(x_0) = \lim_{n\to\infty}\ln\left|\frac{d}{dx}\overbrace{\Psi_N(x_{n+1},\alpha,\varepsilon)\circ\Psi_N\ldots.\circ\Psi_N(x_K,\alpha,\varepsilon)}^{n}\right| = \lim_{n\to\infty}\sum_{k=0}^{n-1}\ln\left|\frac{d\Psi_N(x_k,\alpha,\varepsilon)}{dx}\right|, \tag{9}$$

where $x_k = \overbrace{\Psi_N\circ\Psi_N\circ\ldots.\circ\Psi_N(x_0)}^{k}$. There are three possibilities:

- If $\Lambda < 0$, trajectories go close to each other → stable radial oscillation.
- If $\Lambda = 0$, the orbits maintain their relative positions, they are on a stable attractor.
- If $\Lambda > 0$, the orbits never falls within the basin of attraction of any periodic orbits → unstable radial oscillation (chaotic behavior).

For the values of parameters $\alpha$ and $\varepsilon$, such that the deformed map $\Psi_N$ be measurable, the Birkhoff ergodic theorem implies that the equality of KS entropy and the Lyapunov number, that is:

$$h(\mu,\Psi_n) = \Lambda(x_0,\Psi_N), \tag{10}$$

Combining the analytic results of KS entropy Eq. (8) and SRB measure (Eq. (B.10)) with the Lyapunov characteristic exponents obtained by numerical simulation, we deduce that these $q$-deformed maps are ergodic in certain values of their parameters ($\alpha$ and $\varepsilon$) as the Birkhoff ergodic theorem predicts.

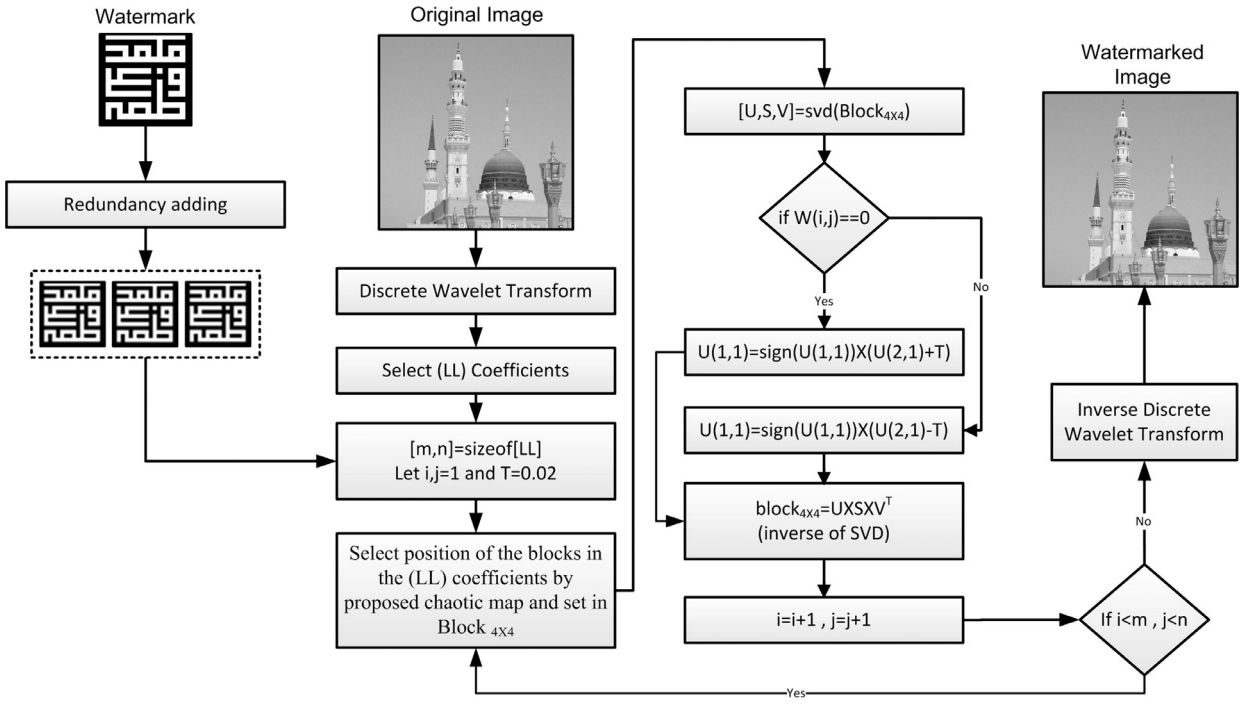


**Fig. 4.** The flowchart of the proposed embedding process.

## 4. Watermarking algorithm

There are two important properties for the performance of chaos based watermarked systems, fixed interval and ergodicity of chaotic orbits, which most of the unimodal maps are lacking [38–41]. In order to avoid these lacks, the $q$-deformed maps are suggested as ratios of polynomials of degree $N$. For first time in this paper, we use the concept of $q$-deformed chaotic maps with an invariant measure, for increasing the security of discrete chaotic watermarking. Certain characteristics of our proposed watermarking method which make it distinctive compared to the other schemes, can be stated as follows:

- Have a large key space: It is clear that the complexity of attack is determined by the verification complexity of each key and the size of the key space.
- Have a large number of fully developed chaotic maps ($q$-deformed maps are defined as ratios of polynomials of degree $N$).
- Having interesting property of being ergodic in certain values of their parameter and in complementary interval of parameter they have only a single period one attractive fixed point. Also, all n-cycles except for possible period one fixed point are unstable.
- Having high complexity due to high chaoticity and flexibility in attributing different values to the control parameters $\alpha$ and $\varepsilon$. Advantage of using two parameters ($\alpha$ and $\varepsilon$) is for computational complexity goal and the structure of the watrmarked system for diffusion. So that, these parameters can be used as secret keys as well.

Furthermore, the efficiency of searching-based chaotic watermarked system which are based on unimodal maps critically dependent on the invariant measure associated with the orbits of the chaotic map. In this sense, the $q$-deformed maps are a good alternative which has an invariant measure for all values of their parameters ($\alpha$ and $\varepsilon$) as the Birkhoff ergodic theorem predicts.

In following the framework of our proposed algorithm is described. The embedding process diagram is shown in Fig. 4 and the process of extraction of the logo also shown in Fig. 5 . Rests of the paper explain the embedding and extraction process of the proposed algorithm.

### 4.1. Watermarking embedding process

In this section the algorithm of embedding are discussed. The watermark logo encryption can be done through the following steps:

- *Step1*: Input: cover image,
- *Step2*: By considering the DWT cover image is converted to the frequency domain,
- *Step3*: Sub-band coefficients are selected,
- *Step4*: Input: logo,
- *Step5*: The logo image for next processes is clones 3 times with redundancy adding process and store in variable $W$ (An advantage of many logos in watermarking process is the possibility to analyze and control their spectral properties),
- *Step6*: Where $T$ is threshold value ($T = 0.015$). The size of the logo is denoted by variables ($m$, $n$) and coordinate ($i$, $j$) of watermark pixel is selected by (1, 1),
- *Step7*: Location of the block in the cover image for the embedding process is selected by pseudo random number generator (Eq. (2)) based on cellular automat and stores in the variable block.
- *Step8*: SVD transform on the blocks with size $4 \times 4$ pixel is done and $U$, $S$, $V$ coefficients are extracted,
- *Step9:* $U(1, 1)$ coefficients is updated as follow:

$$\begin{cases} U(1,1) = sign(U(1,1) * (U(2,1) + T)) & \text{If } W(i,j) = 1 \\ U(1,1) = sign(U(1,1) * (U(2,1) - T)) & \text{If } W(i,j) = 0 \end{cases} \tag{11}$$

- *Step10*: Inverse of SVD is computed to obtain block pixels as follow:

$$Block_{[4\times4]} = U \times S \times V^T \tag{12}$$

- *Step11*: Increase value of the $i$ and $j$,

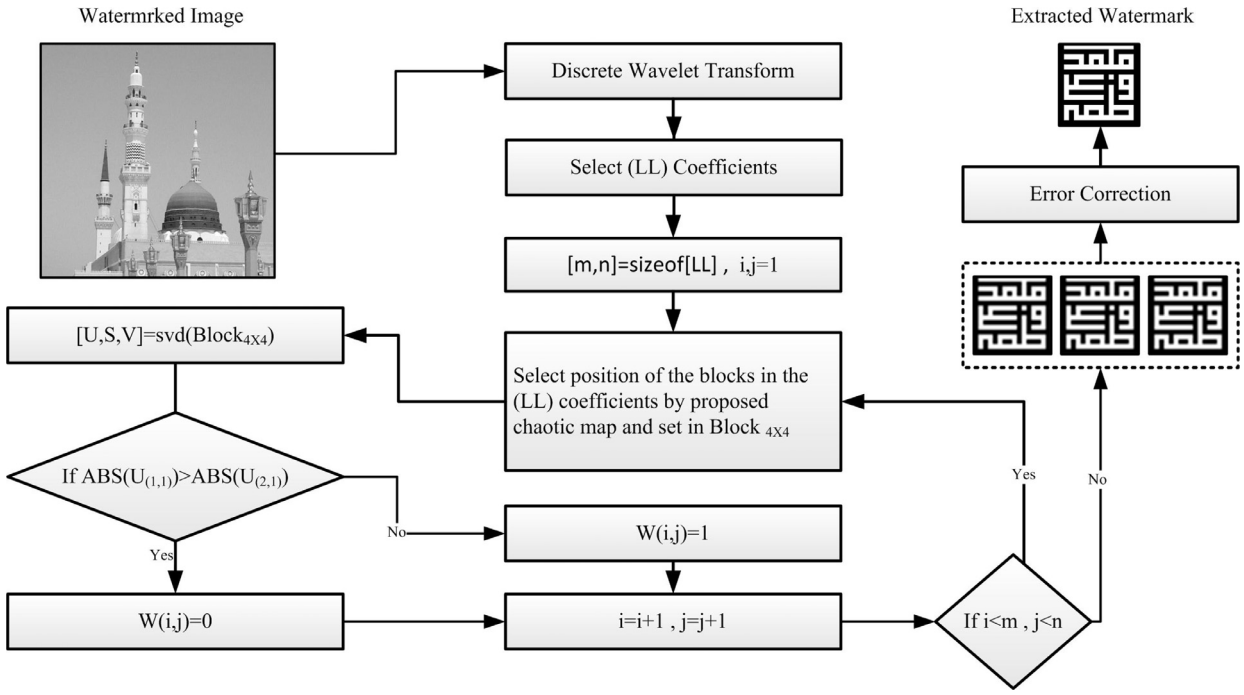


**Fig. 5.** The flowchart of proposed extraction process.

- *Step12*: If $i < m$ and $j < n$ then go to step 7 else go to step 13,
- *Step13*: Do the inverse discrete wavelet transform,
- *Step14*: The final result is the watermarked image.

### 4.2. Watermarking extraction process

Watermark extraction process is very similar to the embedding process. This process consists of the following major parts:

- *Step1*: Input watermarked image,
- *Step2*: The size of the logo $[m \times n]$ inputted and stores in variable $W$ with size $[m \times 3n]$,
- *Step3*: Watermarked image is transferred to the frequency domain with discrete wavelet transform,
- *Step4*: Coefficients related to the selected sub-band are selected,
- *Step5*: Initialize $i, j$ with the value 1,
- *Step6*: Location of the block in the cover image for the embedding process selected by pseudo random number generator (Eq. 2) based on cellular automat and stores in the variable block,
- *Step7*: SVD transform on the blocks with size $4 \times 4$ pixel done and $U, S, V$ coefficients extracted,
- *Step8*: If $|U(1, 1)| > |U(2, 1)|$ go to step 9 and else go to step 10,
- *Step9*: The value of the $W(i, j) = 1$ go to step 11,
- *Step10*: The value of the $W(i, j) = 0$ go to step 11,
- *Step11*: Increase one unit $i$ and $j$ value,
- *Step12*: If $i < m$ and $j < n$ then go to step 6 else go to step 13,
- *Step13*: Extracted logo has a picture contain 3 same logos beside each other,
- *Step14*: Extracted logos (3 logo) compared pixel by pixel and which pixel that have more frequency, selected for creating a final logo. This step is an error correction step,
- *Step15*: Final logo is created and extracted.

## 5. Experimental results

In this section the experimental results of our proposed scheme are discussed to demonstrate the efficiency of the proposed watermarking algorithm. The performance of the proposed method by considering the nine standard gray scale pictures (Lena, Zelda, baboon, camera man,...) and one sample picture "MADINEH" has been tested. The image size selected as $512 \times 512$ pixels. Logo with size $32 \times 32$ in binary form have been added to the pictures. This section is a review of the visual quality measures and the overview of attacks in introduced pictures, also we compare the results with other methods.

### 5.1. Visual quality measures

The visual performance of the proposed method from an aspect of visual quality, impeccability and quality of extracting logo in this paper by considering, Peak Signal to Noise Ratio (PSNR), Bit Error Rate (BER) and Normalized Correlation (NC) evaluated.

#### 5.1.1. Peak signal to noise ratio

This measure shows the effect of the embedding algorithm and noises on the cover image. PSNR measured by the decibel (dB) unit in the range 20 dB (low quality) to 40 dB (high quality). PSNR for Gray scale images defined as,

$$PSNR = 10 \times \log_{10} \frac{255^2}{MSE}(dB), \tag{13}$$

where

$$MSE = \frac{1}{M \times N} \sum_{i=1}^{M} \sum_{j=1}^{N} (H_{i,j} - \acute{H}_{i,j}). \tag{14}$$

it denotes the mean square error between the original image and watermark image. In this equation, $H_{i,j}$ and $\acute{H}_{i,j}$ are value of pixels in the position $(i, j)$ in the cover image and watermark image respectively, and $M \times N$ is the size of the image. The value of the PSNR for the proposed method is shown in Table. 1 for standard test images. In this table proposed method compares with similar methods like [42,43]. The results show the advantage of the proposed method in most test images.

**Table 1**
The PSNR (dB) results for different watermarked images.

| Image name | Proposed method |
|---|---|
| Lena | 40.89 |
| Baboon | 38.45 |
| Barbara | 36.95 |
| Boat | 37.98 |
| Couple | 38.67 |
| F-16g | 38.90 |
| Goldhill | 40.67 |
| Peppers | 40.08 |
| Zelda | 43.58 |

*5.1.2. Bit Error Rate and Normalized Corrolation*

The quality of the extracted logo from the cover image, evaluate by BER and NC measure. BER defined with the following formula:

$$BER = \frac{B}{M \times N} \times 100 \tag{15}$$

where $B$ is the number of detected error on extracted logo. In this measure, zero means that the embedding algorithm doesn't have any effect on the logo. Also, NC is defined by the following formula,

$$NC = \frac{1}{W_h \times W_w} \sum_{i=0}^{W_h-1} \sum_{j=0}^{W_w-1} w(i,j) \times \hat{w}(i,j) \tag{16}$$

Where $W_h$ and $W_w$ are height and width of the watermarked image respectively. $w(i, j)$ is declare the inserted logo and $\hat{w}(i, j)$ is shows the extracted logo. One is the best value for $NC$ and it shows the inserted logo extracted without any distortion. The obtained results of exams presented in Tables. 2 and 3, and compared with [42,44]. Therefore, there is no obvious perceptual distortion between watermarked image and original one; the embedded watermark does not degrade the quality of the original host image. We have to use the same parameters for attacks in order to have a valid comparison. Tables shows the good performance of the proposed method against attacks such as compression, scaling and various types of filtering Table 4.

*5.2. Robustness against attacks*

Stirmark is a powerful tool for measuring and testing the robustness of watermarking algorithms. In this study by considering Stirmark benchmark [45] including the geometric and non-geometric attacks the robustness of watermarking algorithms has been examined. Tests includes:

- JPEG compression: It is a universal format of compression in the images [46,47].
- Median filtering: Median filter is a filter that replaces median of the neighboring pixels to the input pixel [48].
- Low-pass filtering: It is a filter that passes (attenuates) signals with a frequency lower (higher) than a certain cutoff frequency [49].
- Gamma correction: It is the name of a nonlinear operation used to code and decode luminance or tristimulus values in image[49].
- Blurring: Blurring is used in preprocessing steps, such as the removal of small details from an image prior to (large) object extraction, and bridging of small gaps in lines or curves. Noise reduction can be accomplished by blurring [49].
- Sharpening: Process of enhancing the detail of the image to clarify the image.
- Histogram equalization: Histogram equalization is a method in image processing of contrast adjustment by using the image's histogram [49,50].

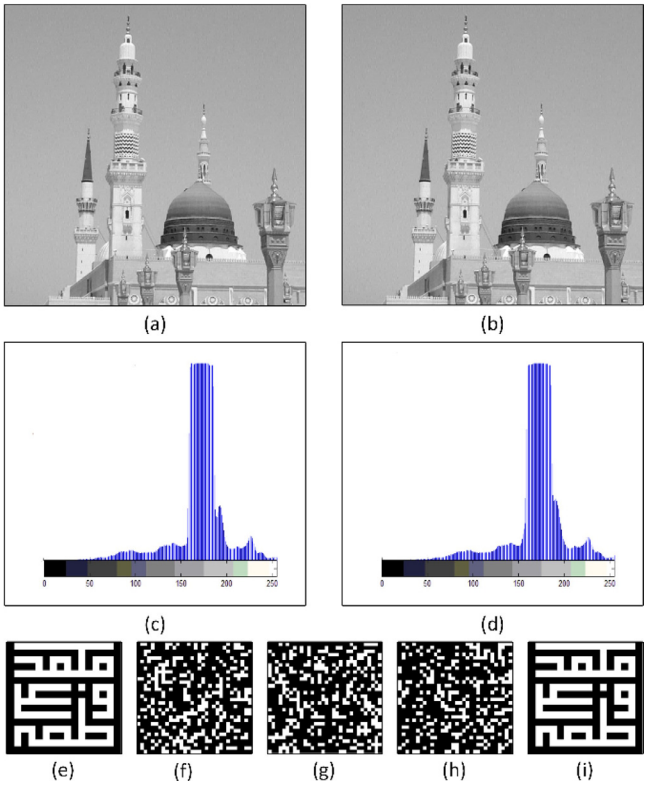


**Fig. 6.** (a) Original image (b) Watermarked image (c) Histogram of original image (d) histogram of watermarked image (e) original watermark logo (f-h) extracted watermark with incorrect keys and (g) correct keys (Left to right to each mode).

Geometric attacks include below items:

- Rotation: Rotation of an input image about an arbitrary pivot point and can be accomplished by translating the origin of the image to the pivot point, performing the rotation, and then translating back by the first translation offset [49].
- Gaussian noise: Gaussian noise is a statistical noise that has a probability density function of normal distribution [50].
- Salt & pepper noise: Salt and pepper noise is a form of noise that represents itself as randomly occurring white and black pixels [49].
- Cropping: This attack is the process to cut part of an image on different size and shape [51,52].

In Fig. 6 we present some example of introduced attacks. The corresponding extracted watermark have been shown in Fig. 7. Also, the test obtained results are presented in Tables 2 and 3.

## 6. Security analysis

When a new image watermarking algorithm is proposed, it should always be accompanied by some security analyses. A good watermarking procedure should be robust against all kinds of attacks. In the following, some security analyses have been performed on the proposed algorithm, which indicated a high security level of the new scheme Fig. 8.

*6.1. Key space*

The key space size is the total number of different keys that can be used in the encryption. It might be defined in term of positive entropy. Actually, key space can be generated by the initial conditions and control parameters of $q$-deformed chaotic maps. A positive way to describe the key space [53] might be in terms of pos-

**Table 2**
Experimental Bit Error Rate (BER) results for Stirmark attacks (%).

| Attacks name | Madineh | Lena | Baboon | Attacks name | Madineh | Lena | Baboon |
|---|---|---|---|---|---|---|---|
| AFFINE-2 | 32.12 | 38.08 | 35.15 | PSNR (30%) | 0.00 | 0.00 | 0.00 |
| AFFINE-4 | 50.78 | 46.28 | 48.04 | PSNR (50%) | 0.00 | 0.00 | 0.00 |
| AFFINE-6 | 54.00 | 47.25 | 44.23 | PSNR (70%) | 0.00 | 0.00 | 0.00 |
| AFFINE-8 | 50.39 | 46.09 | 40.91 | PSNR (90%) | 0.00 | 0.00 | 0.00 |
| CONV-1 | 46.77 | 29.56 | 26.36 | PSNR (100%) | 0.00 | 0.00 | 0.00 |
| CONV-2 | 0.19 | 0.68 | 1.85 | RESC 50 | 0.00 | 0.00 | 0.00 |
| JPEG (15%) | 0.97 | 12.89 | 4.39 | RESC 75 | 0.00 | 0.09 | 0.00 |
| JPEG (20%) | 0.09 | 3.90 | 1.26 | RESC 90 | 0.00 | 0.29 | 1.56 |
| JPEG (40%) | 0.00 | 0.00 | 0.00 | RML 10 | 0.09 | 0.58 | 0.87 |
| JPEG (60%) | 0.00 | 0.00 | 0.00 | RML 30 | 0.19 | 0.68 | 1.36 |
| JPEG (80%) | 0.00 | 0.00 | 0.00 | RML 50 | 0.00 | 0.58 | 1.75 |
| JPEG (100%) | 0.00 | 0.00 | 0.00 | RML 70 | 0.09 | 0.68 | 2.63 |
| LATEST. 0.95 | 47.46 | 54.00 | 50.29 | RML 80 | 0.00 | 2.14 | 3.61 |
| LATEST. 1.1 | 49.70 | 53.71 | 49.41 | RML 90 | 0.00 | 0.68 | 1.46 |
| LATEST. 1.05 | 48.53 | 51.75 | 51.66 | RML 100 | 0.00 | 0.39 | 1.17 |
| LATEST. 1 | 49.12 | 53.12 | 51.66 | RNDDIST 0.95 | 49.60 | 52.53 | 49.21 |
| MEDIAN [3 × 3] | 0.19 | 1.26 | 5.07 | RNDDIST 1.1 | 49.12 | 52.92 | 52.63 |
| MEDIAN [5 × 5] | 25.68 | 37.59 | 38.67 | RNDDIST 1.05 | 47.94 | 52.83 | 52.44 |
| MEDIAN [7 × 7] | 49.51 | 50.09 | 49.41 | RNDDIST 1 | 47.46 | 52.44 | 49.90 |
| MEDIAN [9 × 9] | 40.77 | 50.78 | 49.90 | ROT (0.5°) | 0.09 | 0.19 | 0.68 |
| NOISE (0%) | 0.00 | 0.00 | 0.00 | ROT (1°) | 0.09 | 0.19 | 0.68 |
| NOISE (20%) | 35.74 | 39.25 | 40.72 | ROT (2°) | 0.19 | 0.39 | 0.67 |
| NOISE (40%) | 42.67 | 44.04 | 42.96 | ROT (5°) | 0.19 | 0.49 | 0.39 |
| NOISE (80%) | 46.48 | 49.41 | 45.99 | ROT (15°) | 0.58 | 1.07 | 1.07 |
| PSNR (0%) | 0.00 | 0.00 | 0.00 | ROT (45°) | 1.07 | 2.66 | 1.49 |
| PSNR (10%) | 0.00 | 0.00 | 0.00 | ROT (90°) | 0.00 | 0.00 | 0.00 |
| Blurring | 0.48 | 1.66 | 1.75 | Gamma Cor. | 3.90 | 3.80 | 0.97 |
| Hist. Equalization | 0.00 | 0.00 | 0.09 | Complement | 100 | 100 | 100 |
| Low Pass Filter | 0.00 | 0.00 | 0.00 | Sharpening | 0.19 | 0.78 | 1.75 |
| Salt and Paper (5%) | 0.78 | 1.56 | 1.46 | | | | |

**Table 3**
Experimental PSNR results for Stirmark attacks (dB).

| Attacks name | Madineh | Lena | Baboon | Attacks name | Madineh | Lena | Baboon |
|---|---|---|---|---|---|---|---|
| AFFINE-2 | 14.97 | 16.48 | 14.81 | PSNR (30%) | 29.59 | 29.66 | 29.68 |
| AFFINE-4 | 14.82 | 15.17 | 15.25 | PSNR (50%) | 25.67 | 25.69 | 25.70 |
| AFFINE-6 | 17.71 | 19.29 | 17.44 | PSNR (70%) | 22.94 | 22.94 | 22.94 |
| AFFINE-8 | 18.29 | 20.15 | 17.66 | PSNR (90%) | 20.86 | 20.84 | 20.85 |
| CONV-1 | 9.85 | 8.73 | 8.30 | PSNR (100%) | 20.15 | 20.13 | 20.13 |
| CONV-2 | 4.46 | 6.81 | 6.70 | RESC 50 | 25.67 | 25.60 | 25.55 |
| JPEG (15%) | 35.11 | 34.59 | 32.38 | RESC 75 | 25.67 | 25.66 | 25.65 |
| JPEG (20%) | 36.23 | 35.53 | 33.71 | RESC 90 | 25.53 | 25.58 | 25.07 |
| JPEG (40%) | 38.56 | 37.00 | 36.24 | RML 10 | 25.49 | 25.55 | 25.28 |
| JPEG (60%) | 38.48 | 37.81 | 37.46 | RML 30 | 25.44 | 25.55 | 25.19 |
| JPEG (80%) | 38.58 | 38.94 | 38.66 | RML 50 | 25.43 | 25.52 | 25.19 |
| JPEG (100%) | 39.05 | 40.03 | 40.17 | RML 70 | 25.36 | 25.48 | 25.13 |
| LATEST. 0.95 | 16.58 | 6.40 | 10.88 | RML 80 | 25.28 | 25.46 | 24.13 |
| LATEST. 1.1 | 16.11 | 6.28 | 10.27 | RML 90 | 25.46 | 25.57 | 25.24 |
| LATEST. 1.05 | 16.25 | 6.32 | 10.41 | RML 100 | 25.46 | 25.55 | 25.24 |
| LATEST. 1 | 16.41 | 6.35 | 10.54 | RNDDIST 0.95 | 24.42 | 28.28 | 28.08 |
| MEDIAN [3 × 3] | 25.08 | 25.00 | 24.27 | RNDDIST 1.1 | 24.19 | 27.87 | 27.74 |
| MEDIAN [5 × 5] | 24.89 | 25.22 | 24.21 | RNDDIST 1.05 | 24.26 | 28.00 | 27.85 |
| MEDIAN [7 × 7] | 24.51 | 25.18 | 23.35 | RNDDIST 1 | 24.62 | 28.13 | 27.96 |
| MEDIAN [9 × 9] | 23.95 | 25.00 | 22.30 | ROT (0.5°) | 23.09 | 24.88 | 19.14 |
| NOISE (0%) | 39.05 | 40.89 | 38.45 | ROT (1°) | 20.32 | 21.14 | 17.37 |
| NOISE (20%) | 6.72 | 8.43 | 8.25 | ROT (2°) | 18.06 | 18.06 | 16.57 |
| NOISE (40%) | 5.31 | 6.89 | 6.80 | ROT (5°) | 14.64 | 14.46 | 14.49 |
| NOISE (80%) | 4.75 | 6.17 | 6.15 | ROT (15°) | 12.07 | 11.57 | 12.32 |
| PSNR (0%) | 39.39 | 40.10 | 40.24 | ROT (45°) | 10.05 | 10.45 | 10.69 |
| PSNR (10%) | 35.96 | 36.28 | 36.34 | ROT (90°) | 16.61 | 11.17 | 13.26 |
| Blurring | 27.79 | 30.61 | 23.10 | Gamma Cor. | 12.37 | 14.92 | 14.62 |
| Hist. Equalization | 11.15 | 19.01 | 17.08 | Complement | 7.92 | 8.49 | 9.97 |
| Low Pass Filter | 40.14 | 40.90 | 40.74 | Sharpening | 28.72 | 29.78 | 27.53 |
| Salt and Paper (5%) | 25.23 | 25.35 | 25.40 | | | | |

**Table 4**
The key space analysis of q-deformed map .

| q-deformed parameters | best range | precision (float) | precision (binary bit) |
|---|---|---|---|
| X | [0,1] | $10^{-14}$ | 47 |
| $\alpha$ | [0.5,2] | $10^{-14}$ | 47 |
| $\varepsilon$ | [0,1] | $10^{-14}$ | 47 |
| key space | | $47+47+47 = 141$ bit | |

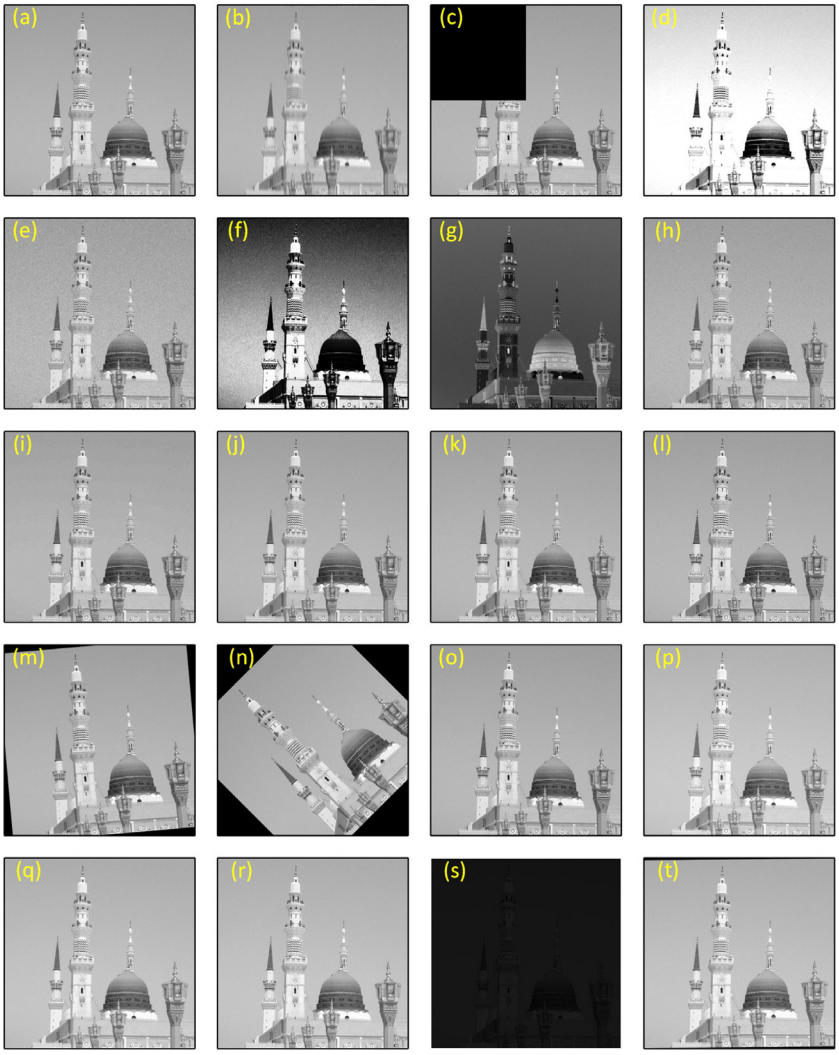


**Fig. 7.** The corresponding best Extracted watermarks for denoted attacks. (a) Jpeg Compression (70%) , (b) Motion blur (45°) , (c) Cropping (25%), (d)Histogram Equalization, (e) Gaussian noise (0, 0.01) , (f) Sharpening, (g) Complement , (h) Salt & Pepper noise 10% , (i) Median filter [3 × 3], (j) Jpeg Compression (60%) , (k) Jpeg Compression (50%) , (l) Jpeg Compression (40%) (m) Rotation (5°) (n) Rotation (45°) (o)Low-pass filter [5 × 5], (p) RESC 50, (q) RESC 75, (r) RML 10 (s) Gamma Correction (t)AFFINE 1 (Left to right to each mode).

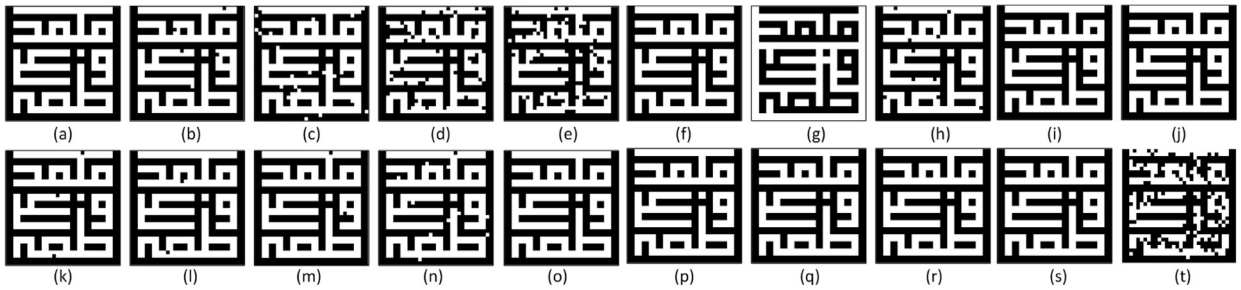


**Fig. 8.** The corresponding best Extracted Logo for denoted attacks. (a) Jpeg Compression (70%) , (b) Motion blur (45°) , (c) Cropping (25%), (d)Histogram Equalization, (e) Gaussian noise (0, 0.01) , (f) Sharpening, (g) Complement , (h) Salt & Pepper noise 10% , (i) Median filter [3 × 3], (j) Jpeg Compression (60%) , (k) Jpeg Compression (50%) , (l) Jpeg Compression (40%) (m) Rotation (5°) (n) Rotation (45°) (o)Low-pass filter [5 × 5], (p) RESC 50, (q) RESC 75, (r) RML 10 (s) Gamma Correction (t)AFFINE 1 (Left to right to each mode).

itive Lyapunov exponents. By considering the suitable control parameters domain (in positive Lyapunov exponents) this space generated (See Fig. 6). High level security domain begin with $2^{128}$ [14]. Here, the key space is large enough to resist all kinds of brute-force attacks [53,54]. In our proposed method, by considering the control parameters, initial condition and $q$-parameter is computed as below:

$$T(x_0, \alpha, \varepsilon) = \theta(X_0 \times \alpha \times \varepsilon) \tag{17}$$

Where $\epsilon \in [0, 1]$ , $x_0 \in [0, 1] (x_0 \in [0, \infty))$, and for control parameter $\alpha$, in selected example (Eq. (2)) is varying in $\alpha \in [\frac{1}{2}, 2)$. It is listed in Table. 1.

**Table 5**
The 800-22 test result of.

| Statistical Test | $p$-value | Result |
|---|---|---|
| Frequency Test | 0.6227 | Success |
| Block Frequency Test (m = 128) | 0.7051 | Success |
| Cumulative-Forward | 0.2530 | Success |
| Cumulative-Reverse | 0.5966 | Success |
| Run Test | 0.5607 | Success |
| Long Runs of Ones | 0.5632 | Success |
| Rank | 0.9635 | Success |
| Spectral DFT | 0.5421 | Success |
| Non-Overlapping Temp.(m = 9,B = 000000001) | 0.0626 | Success |
| Overlapping Temp. (m = 9) | 0.9906 | Success |
| Universal | 0.7690 | Success |
| Approximation Entropy (m = 10) | 0.0000 | Success |
| Random Excursions (X = −4) | 0.0266 | Success |
| Random Excursions (X = −2) | 0.9621 | Success |
| Random Excursions (X = −1) | 0.9699 | Success |
| Random Excursions (X = 1) | 0.9958 | Success |
| Random Excursions (X = 2) | 0.9426 | Success |
| Random Excursions (X = 4) | 0.9665 | Success |
| Random Excursions Variant (X = −8) | 0.7084 | Success |
| Random Excursions Variant (X = −6) | 0.8146 | Success |
| Random Excursions Variant (X = −4) | 0.5498 | Success |
| Random Excursions Variant (X = −2) | 0.6422 | Success |
| Random Excursions Variant (X = −1) | 0.5198 | Success |
| Random Excursions Variant (X = 1) | 0.4210 | Success |
| Random Excursions Variant (X = 2) | 0.6759 | Success |
| Random Excursions Variant (X = 4) | 0.9757 | Success |
| Random Excursions Variant (X = 6) | 0.7463 | Success |
| Random Excursions Variant (X = 8) | 0.7553 | Success |
| Serial (m = 16, $\nabla\psi_m^2$) | 0.2010 | Success |
| Linear Complexity (M = 500) | 0.5563 | Success |

### 6.2. Random number test

Encryption process requiring the generation of random numbers. Random number generators are based on specific mathematical algorithms. In this study by considering the hierarchy of $q$-deformed maps an effective way to generate random numbers uniformly distributed on the interval [0, 1] is introduced. This family could provide the series with good distribution, long period and portability, which is common properties of good random number generators. We have used National Institute of Standard and Technology statistical test (NIST) [55] to examine the quality of our proposed algorithm based on $q$-deformed chaotic maps (Eq. (2)). Where it could produced the random sequences by deterministic processes. As it was shown in Table 5, they could pass all of the statistical tests, such as frequency, block frequency, cumulative sums, runs, longest run, rank, and fast Fourier transform (FFT). In NIST 800-22 tests, if $p$-value $> 0.01$, then the PRNG passes this test, naturally the larger $p$-value is present the larger randomness.

## 7. Summary

In this paper, a scheme for $q$-deformed (according to the scheme suggested by Jaganathan et al.[28]) based on the hierarchy of chaotic maps is proposed. We particularly expand upon previously reported results of a hierarchy of dynamical systems [56,57], for construction of a new hierarchy of $q$-deformation maps with an invariant measure. These maps have advantages such as ergodicity and the possibility of KS entropy calculation. In these maps the control parameter is switched to $q$-deformation control parameter and parameter $\alpha$. Consequently, the hierarchy of $q$-deformation maps have richer dynamical phenomena than the canonical hierarchy of chaotic maps and all the features of the canonical chaotic maps can be accessed via changing the deformation parameters ($q$) and without varying the values of the parameter $\alpha$.

Finally, a new watermarking scheme for blind digital image watermarking based on $q$-deformed chaotic maps and DWT (powerful mathematical transforms) was proposed. These $q$-deformed maps was implemented to increase both the number of keys and complexities involved in the algorithm. Furthermore, the $q$-deformation control parameter and the initial values of $q$-deformed maps are deemed as necessary keys for correctly restituting watermarks, which greatly enhanced the system security. The experimental results have demonstrated the extracted watermark logo had very good quality. In addition to some features aforesaid, the most important advantage of these $q$-deformation maps is the existence of the two parameters, $\alpha$ and $\varepsilon$. It seems that the excellent efficiency of the new watermarking scheme is derived from this property. Moreover, based on all experimental results and analysis, the conclusion is that, from a watermarking viewpoint, the proposed algorithm is a best candidates for practical applications in information security fields.

## Acknowledgment

The authors express their thanks to Dr. P. Ayubi for assistance with DWT and in that line improved the manuscript significantly.

## Appendix A. One parameter families

Hierarchy of one-parameter families of chaotic maps with an invariant measure can be defined as [56]:

$$\Phi(x,\alpha) = \frac{\alpha^2 F}{1+(\alpha^2-1)F}\,. \tag{A.1}$$

where $F$ substitutes with Chebyshev polynomial of type one, $T_N(x)$ for $\Phi_N^{(1)}(x,\alpha)$ and in the case of Chebyshev polynomial of type two, $U_N(x)$ for $\Phi_N^{(2)}(x,\alpha)$. As an example, some of these maps are given below:

$$\Phi_2^{(1)} = \frac{\alpha^2(2x-1)^2}{4x(1-x)+\alpha^2(2x-1)^2},\quad \Phi_2^{(2)} = \frac{4\alpha^2 x(1-x)}{1+4(\alpha^2-1)x(1-x)},$$
$$\Phi_3^{(1)} = \Phi_3^{(2)} = \frac{\alpha^2 x(4x-3)^2}{\alpha^2 x(4x-3)^2+(1-x)(4x-1)^2}. \tag{A.2}$$

We have derived analytically their invariant measure for arbitrary values of the parameter $\alpha$ and any integer values of $N$:

$$\mu_{\Phi_N^{(1,2)}(x,\alpha)}(x,\beta) = \frac{1}{\pi}\frac{\sqrt{\beta}}{\sqrt{x(1-x)}(\beta+(1-\beta)x)}\,. \tag{A.3}$$

with $\beta > 0$ is the invariant measure of the maps $\Phi_N^{(1,2)}(x,\alpha)$ provided that, we choose the parameter $\alpha$ in the following form:

$$\alpha = \begin{cases} \dfrac{\sum_{k=0}^{[\frac{(N-1)}{2}]} C_{2k+1}^N \beta^{-k}}{\sum_{k=0}^{[\frac{N}{2}]} C_{2k}^N \beta^{-k}} & \text{for} \quad \text{odd values of } N \\ \dfrac{\beta\sum_{k=0}^{[\frac{(N)}{2}]} C_{2k}^N \beta^{-k}}{\sum_{k=0}^{[\frac{(N-1)}{2}]} C_{2k+1}^N \beta^{-k}} & \text{for} \quad \text{even values of } N \end{cases} \tag{A.4}$$

where the symbol [ ] means the greatest integer part.

## Appendix B. Invariant measure

There are various methods to find invariant measures [37]. We focus on the Stieltjes transform approach to calculate the SRB measure [58]. Invariant measures remain unaffected by dynamics, so they are fixed points of the PF-operator, with the unit eigenvalue:

$$\mathcal{L}^t\mu(x) = \int_M \delta(x-\Psi^t(y))\mu(y) = \mu(x) \tag{B.1}$$

Depending on the choice of $\Psi^t(x)$, there may be no, one, or many solutions of the eigenfunction condition. Now, by considering

$d\mu(y) = \delta(y - \Psi(x))d\nu(x)$ the density at the $n^{th}$ time becomes:

$$y^n d\mu(y) = \delta(y - \Psi(x))y^n d\nu(x). \tag{B.2}$$

By integrating Eq. (B.2), we have:

$$\int_a^b y^n d\mu(y) = \int_a^b \delta(y - \Psi(x))y^n d\nu(x) = \int_a^b (\Psi(x))^n d\nu(x). \tag{B.3}$$

that can be presented in the following form either:

$$\mu_n = \int_a^b x^n d\mu = \int_a^b (\Psi(x))^n d\mu. \tag{B.4}$$

The spectral distribution can be determined in the last step in terms of $x_l$, based on the following equation (for more details see Ref.[37,59]):

$$\mu = \sum_l A_l \delta(x - x_l). \tag{B.5}$$

According to the proposed steps in the Ref. [60], and also in order to calculate the invariant measure for $\Psi_2(x, \alpha, \varepsilon)$, we calculate the moments:

$$\begin{aligned}\mu_n = &\left(\frac{4\alpha^2\big((\varepsilon+2)^2 - 4\alpha^2(1+\varepsilon)\big)(1+\varepsilon)(1+\gamma(\varepsilon,\alpha))}{\gamma(\varepsilon,\alpha)^2 - \gamma(\varepsilon,\alpha)\chi(\varepsilon,\alpha)}\right)^n \\ &\times \sum_{k=0}^{n}\left(\frac{\gamma(\varepsilon,\alpha)+\chi(\varepsilon,\alpha)\gamma(\varepsilon,\alpha)}{\chi(\varepsilon,\alpha)+\chi(\varepsilon,\alpha)\gamma(\varepsilon,\alpha)}\right)^k \\ &\times (-1)^{n-k}C_k^n \sum_{k'=0}^{n-k}(-1)^{k'}C_{k'}^{n-k+k'-1}\left(\frac{1}{\gamma(\varepsilon,\alpha)}\right)^{k'} \\ &\times \sum_{k''=0}^{k} C_{k''}^{k+k''-1}\left(\frac{1}{\chi(\varepsilon,\alpha)}\right)^{k''}\mu_{k'+k''}\end{aligned} \tag{B.6}$$

where $\mu_{k'+k''} = \int_0^1 x^{k'+k''}d\mu(x)$ and for $n = 0, 1, 2, \ldots$, $k = 0, 1, 2, \ldots$ we find

$$\begin{cases}\gamma(\varepsilon,\alpha) = \dfrac{(-\varepsilon - 2 + 2\alpha^2 + 2\sqrt{\alpha^2-\alpha^4})(1+\varepsilon)}{(\varepsilon+2)^2 - 4\alpha^2(1+\varepsilon)} \\ \chi(\varepsilon,\alpha) = \dfrac{(-\varepsilon - 2 + 2\alpha^2 - 2\sqrt{\alpha^2-\alpha^4})(1+\varepsilon)}{(\varepsilon+2)^2 - 4\alpha^2(1+\varepsilon)}\end{cases} \tag{B.7}$$

It should be assumed that, $\mu_n = 0$ for all odd value of $n$ . As an example by considering the first five moments:

$$\begin{aligned}\mu_0 &= 1, \\ \mu_2 &= \frac{\big(4\alpha^2(1+\varepsilon)\big((\varepsilon+2)^2 - 4\alpha^2(1+\varepsilon)\big)\big)^2}{\chi^2 - \gamma^2 - \frac{\alpha^2}{1-\alpha^2}\big((\varepsilon+2)^2 - 4\alpha^2(1+\varepsilon)\big)^4\left(\frac{3\chi^2(1+\gamma)^2}{\gamma^2} + (1+\chi)(\gamma+4)\right)}, \\ \mu_4 &= \frac{\left(\frac{4\alpha^2(1+\varepsilon)((\varepsilon+2)^2 - 4\alpha^2(1+\varepsilon))(1+\gamma)(\gamma-\chi)}{\gamma}\right)^4}{(\gamma-\chi)^4 - \frac{1+\chi}{1+\gamma}\big(4\alpha^2(1+\varepsilon)(1+\gamma)\big)^4\left(\frac{35}{\gamma^6} - \frac{80}{\chi^2\gamma^6} + \frac{24(1+\chi^2)(1+\gamma)}{\chi^4(1+\gamma^2)\gamma^4(1+\chi)} - \frac{80}{\gamma^6\chi^4} + \frac{35}{\chi^8}\right)} \\ &\quad + \frac{\left(\frac{4\alpha^2((\varepsilon+2)^2-1)(1+\varepsilon)(1+\gamma)}{\gamma^2-\gamma\chi}\right)^4\mu_2\left(\frac{10}{\gamma^2} - \frac{4(\gamma+\gamma\chi)}{\chi+\gamma\chi}\left(\frac{3}{\gamma\chi} + \frac{6}{\gamma^2}\right) + 6\left(\frac{\gamma+\gamma\chi}{\chi+\gamma\chi}\right)^2\left(\frac{4}{\gamma\chi} + \frac{3}{\gamma} + \frac{3}{\chi^2}\right)\right)}{1 - \left(\frac{4\alpha^2(1+\gamma)}{\gamma^2-\gamma\chi}\right)^4\left(\frac{35}{\gamma^2} - \frac{80(\gamma+\chi\gamma)}{\chi^2\gamma^3+\chi^2\gamma^4} + \frac{24(\gamma^2+\chi^2\gamma^2)}{\chi^2+\chi^2\gamma^2}\frac{1}{\chi^2\gamma^2} - \frac{80}{\gamma\chi^2}\left(\frac{\gamma+\chi\gamma}{\chi^2\gamma^3+\chi^2\gamma^4}\right) + \frac{35}{\chi^4}\left(\frac{\gamma+\chi\gamma}{\chi+\gamma\chi}\right)^4\right)}\end{aligned} \tag{B.8}$$

At the second step, we calculate the coefficients $\lambda_n$ according to Eq. (8) in Ref. [60]:

$$\begin{aligned}\lambda_1 &= 1, \\ \lambda_2 &= \frac{\big(4\alpha^2(1+\varepsilon)\big((\varepsilon+2)^2 - 4\alpha^2(1+\varepsilon)\big)\big)^2}{\chi^2 - \gamma^2 - \frac{\alpha^2}{1-\alpha^2}\big((\varepsilon+2)^2 - 4\alpha^2(1+\varepsilon)\big)^4\left(\frac{3\chi^2(1+\gamma)^2}{\gamma^2} + (1+\chi)(\gamma+4)\right)}\end{aligned} \tag{B.9}$$

Now, by considering the general form of $P$-polynomial (Eq. (7) in Ref. [60]), we have:

$$P_2(x) = x^2 - \frac{\big(4\alpha^2(1+\varepsilon)\big((\varepsilon+2)^2 - 4\alpha^2(1+\varepsilon)\big)\big)^2}{\chi^2 - \gamma^2 - \frac{\alpha^2}{1-\alpha^2}\big((\varepsilon+2)^2 - 4\alpha^2(1+\varepsilon)\big)^4\left(\frac{3\chi^2(1+\gamma)^2}{\gamma^2} + (1+\chi)(\gamma+4)\right)}$$

In the next step, according to the definition of the Stieltjes transform (Eq. (9) in Ref. [60]), we can write:

$$\begin{aligned}G_\mu(x) &= \frac{1}{x - \frac{\omega_1}{x}} \\ &= \frac{x}{\left(x - \sqrt{\frac{\big(4\alpha^2(1+\varepsilon)\big((\varepsilon+2)^2 - 4\alpha^2(1+\varepsilon)\big)\big)^2}{\chi^2 - \gamma^2 - \frac{\alpha^2}{1-\alpha^2}\big((\varepsilon+2)^2 - 4\alpha^2(1+\varepsilon)\big)^4\left(\frac{3\chi^2(1+\gamma)^2}{\gamma^2} + (1+\chi)(\gamma+4)\right)}}\right)} \\ &\quad \times \frac{1}{\left(x + \sqrt{\frac{\big(4\alpha^2(1+\varepsilon)\big((\varepsilon+2)^2 - 4\alpha^2(1+\varepsilon)\big)\big)^2}{\chi^2 - \gamma^2 - \frac{\alpha^2}{1-\alpha^2}\big((\varepsilon+2)^2 - 4\alpha^2(1+\varepsilon)\big)^4\left(\frac{3\chi^2(1+\gamma)^2}{\gamma^2} + (1+\chi)(\gamma+4)\right)}}\right)}\end{aligned}$$

In the last step, with regard to the relation (Eq. (11) in Ref. [60]), the Guass quadrature constants are shaped as follows:

$$A_l = \frac{1}{2}$$

Now, according to the definition of the invariant measure Eq. (B.5), we can write:

$$\begin{aligned}\mu = &\frac{1}{2}\delta\left(x + \sqrt{\frac{\big(4\alpha^2(1+\varepsilon)\big((\varepsilon+2)^2 - 4\alpha^2(1+\varepsilon)\big)\big)^2}{\chi^2 - \gamma^2 - \frac{\alpha^2}{1-\alpha^2}\big((\varepsilon+2)^2 - 4\alpha^2(1+\varepsilon)\big)^4\left(\frac{3\chi^2(1+\gamma)^2}{\gamma^2} + (1+\chi)(\gamma+4)\right)}}\right) \\ &+ \frac{1}{2}\delta\left(x - \sqrt{\frac{\big(4\alpha^2(1+\varepsilon)\big((\varepsilon+2)^2 - 4\alpha^2(1+\varepsilon)\big)\big)^2}{\chi^2 - \gamma^2 - \frac{\alpha^2}{1-\alpha^2}\big((\varepsilon+2)^2 - 4\alpha^2(1+\varepsilon)\big)^4\left(\frac{3\chi^2(1+\gamma)^2}{\gamma^2} + (1+\chi)(\gamma+4)\right)}}\right)\end{aligned} \tag{B.10}$$

In order to avoid boring the reader with dull calculations, we only present that the variation of measure until second order for the selected example map. It is clear that the more you can increase the amount of $n$, the closer on get the reality. In this case, the infinite invariant measure on $x = 0$ (or $x = 1$) is corresponding to one unstable fixed point. The probability of distribution around the fixed points influenced by the variation of $\varepsilon$ and $\alpha$. Actually, this interesting property is due to the existence of the SRB measure for the range of values of the parameter of these maps.

## References


[1] Cox I, Miller M, Bloom J, Fridrich J, Kalker T. Digital watermarking and steganography. Morgan Kaufmann 2007.
[2] Yüzkollar C, Kocabıçak U. Region based interpolation error expansion algorithm for reversible image watermarking. Appl Soft Comput 2015;33:127–35.
[3] Wang X-Y, Miao E-N, Yang H-Y. A new SVM-based image watermarking using Gaussian–Hermite moments. Appl Soft Comput 2012;12(2):887–903.
[4] Agilandeeswari L, Ganesan K. An adaptive HVS based video watermarking scheme for multiple watermarks using BAM neural networks and fuzzy inference system. Expert Syst Appl 2016.
[5] Thind DK, Jindal S. A semi blind DWT-SVD video watermarking. Procedia Comput Sci 2015;46:1661–7.
[6] Hua G, Huang J, Shi YQ, Goh J, Thing VL. Twenty years of digital audio watermarking a comprehensive review. Signal Process 2016;128:222–42.
[7] Liu S-H, Yao H-X, Gao W, Liu Y-L. An image fragile watermark scheme based on chaotic image pattern and pixel-pairs. Appl Math Comput 2007;185(2):869–82.
[8] Katzenbeisser S, Petitcolas F. Information hiding techniques for steganography and digital watermarking. Artech House; 2000.
[9] Lee Z-J, Lin S-W, Su S-F, Lin C-Y. A hybrid watermarking technique applied to digital images. Appl Soft Comput 2008;8(1):798–808.
[10] Arnold M, Schmucker M, Wolthusen SD. Techniques and applications of digital watermarking and content protection. Artech House 2002.
[11] Sathik MM, Sujatha S. A novel DWT based invisible watermarking technique for digital images.. Int Arab J e-Technol 2012;2(3):167–73.
[12] Mostafa SA, Tolba A, Abdelkader F, Elhindy HM. Video watermarking scheme based on principal component analysis and wavelet transform. Int J Comput SciNetw Secur 2009;9(8):45–52.
[13] Mondal M, Barik D. Spatial domain robust watermarking scheme for color image. Int J Adv Comput Sci 2012;2(1):24–7.
[14] Behnia S, Teshnehlab M, Ayubi P. Multiple-watermarking scheme based on improved chaotic maps. Commun Nonlinear Sci Numer Simul 2010;15(9):2469–78.
[15] Behnia S, Ahadpour S, Ayubi P. Design and implementation of coupled chaotic maps in watermarking. Appl Soft Comput 2014a;21:481–90.
[16] Das C, Panigrahi S, Sharma VK, Mahapatra K. A novel blind robust image watermarking in DCT domain using inter-block coefficient correlation. AEU-Int J ElectronCommun 2014;68(3):244–53.
[17] Huang F, Guan Z-H. A hybrid SVD-DCT watermarking method based on LPSNR. Pattern Recognit Lett 2004;25(15):1769–75.
[18] Ali M, Ahn CW, Pant M, Siarry P. An image watermarking scheme in wavelet domain with optimized compensation of singular value decomposition via artificial bee colony. Inf Sci 2015;301:44–60.
[19] Makbol NM, Khoo BE. A new robust and secure digital image watermarking scheme based on the integer wavelet transform and singular value decomposition. Digit Signal Process 2014;33:134–47.
[20] Lang J, Zhang Z-g. Blind digital watermarking method in the fractional fourier transform domain. Opt Lasers Eng 2014;53:112–21.
[21] Rawat S, Raman B. A blind watermarking algorithm based on fractional Fourier transform and visual cryptography. Signal Process 2012;92(6):1480–91.
[22] Khorrami N, Ayubi P, Behnia S, Ayubi J. A SSVD-chaos digital image watermarking scheme based on multiple chaotic system. In: Signal processing and information technology. Springer; 2014. p. 9–18.
[23] Tsai H-H, Jhuang Y-J, Lai Y-S. An SVD-based image watermarking in wavelet domain using SVR and PSO. Appl Soft Comput 2012;12(8):2442–53.
[24] Vaishnavi D, Subashini T. Image tamper detection based on edge image and chaotic arnold map. Indian J Sci Technol 2015;8(6):548–55.
[25] Castellani L, Wess J. Quantum groups and their applications in physics, 127. IOS Press; 1996.
[26] Wess J. q-deformed Heisenberg algebras. In: Geometry and quantum physics. Springer; 2000. p. 311–82.
[27] Ogievetsky O, Schmidke W, Wess J, Zumino B. q-deformed Poincaré algebra. Commun Math Phys 1992;150(3):495–518.
[28] Jaganathan R, Sinha S. A q-deformed nonlinear map. Phys Lett A 2005;338(3):277–87.
[29] Patidar V. Co-existence of regular and chaotic motions in the gaussian map. Electron J Theor Phys, EJTP3 2006;338(13):29–40.
[30] Patidar V, Sud K. A comparative study on the co-existing attractors in the gaussian map and its q-deformed version. Commun Nonlinear Sci Numer Simul 2009;14(3):827–38.
[31] Patidar V, Purohit G, Sud K. A numerical exploration of the dynamical behavior of q-deformed nonlinear maps. Chaotic Syst 2010:257–67.
[32] Shrimali MD, Banerjee S. Delayed q-deformed logistic map. Commun Nonlinear Sci Numer Simul 2013;18(11):3126–33.
[33] Chen LD, G. Anticontrol of chaos via feedback. Int J Bifurcat Chaos 1998;8:1585–90.
[34] Starkov K, Chen G. Chaotification of polynomial continuous-time systems and rational normal forms. Chaos, Solitons Fractals 2004;22(4):849–56.
[35] Wang XF, Chen G, Yu X. Anticontrol of chaos in continuous-time systems via time-delay feedback. Chaos 2000;10(4):771–9.
[36] Chen H-K, Lee C-I. Anti-control of chaos in rigid body motion. Chaos, Solitons Fractals 2004;21(4):957–65.
[37] Dorfman JR. An introduction to chaos in nonequilibrium statistical mechanics, 14. Cambridge University Press; 1999.
[38] Tefas A, Nikolaidis A, Nikolaidis N, Solachidis V, Tsekeridou S, Pitas I. Markov chaotic sequences for correlation based watermarking schemes. Chaos, Solitons Fractals 2003;17(2):567–73.
[39] Nikolaidis A, Pitas I. Comparison of different chaotic maps with application to image watermarking. In: IEEE international symposium on circuits and systems, vol. 1999. IEEE; 2000. P. V–509.
[40] Tsekeridou S, Solachidis V, Nikolaidis N, Nikolaidis A, Tefas A, Pitas I. Theoretic investigation of the use of watermark signals derived from bernoulli chaotic sequences. In: Proceedings of the Scandinavian conference on image analysis; 2001. p. 600–7.
[41] Behnia S, Ahadpour S, Ayubi P. Design and implementation of coupled chaotic maps in watermarking. Appl Soft Comput 2014b;21:481–90.
[42] Ranjbar S, Zargari F, Ghanbari M. A highly robust two-stage contourlet-based digital image watermarking method. Signal Process Image Commun 2013;28(10):1526–36.
[43] Mohan BC, Kumar SS. Robust digital watermarking scheme using contourlet transform. Int J Comput SciNetw Secur 2008;8(2):43–51.
[44] Lin W-H, Wang Y-R, Horng S-J, Kao T-W, Pan Y. A blind watermarking method using maximum wavelet coefficient quantization. Expert Syst Appl 2009;36(9):11509–16.
[45] Kutter M, Petitcolas FA. Fair benchmark for image watermarking systems. Electronic Imaging'99, International Society for Optics and Photonics; 1999. p. 226–39.
[46] Pennebaker WB, Mitchell JL. JPEG: still image data compression standard. Springer Science & Business Media 1992.
[47] Acharya T, Tsai P-S. JPEG2000 standard for image compression: concepts, algorithms and VLSI architectures. John Wiley & Sons; 2005.
[48] Huang T, Yang G, Tang G. A fast two-dimensional median filtering algorithm. IEEE Trans Acoust 1979;27(1):13–18.
[49] Gonzalez RC, Richard E. Woods, digital image processing. Prentice Hall Press; 2008. ISBN 0-201-18075-8.
[50] Pratt W.K., et al. Digital image processing. (1978).
[51] Lee P, Chenb Y, Pei S, Chena Y. Reply to the comment keystream cryptanalysis of a chaotic cryptographic method. Comput Phys Commun 2004;160:208–14.
[52] Poynton C. Digital video and HD: algorithms and interfaces. Elsevier; 2012.
[53] Schneier B.. Applied cryptography: protocols, algorithms, and source code in C. 1996. 2, 216–222
[54] Ecrypt ii yearly report on algorithms and keysizes. 2010. http://www.ecrypt.eu.org/documents/D.SPA.13.pdf.
[55] National institute of standard and technology statistical test (nist).http://www.nist.gov/.
[56] Jafarizadeh M, Behnia S, Khorram S, Nagshara H. Hierarchy of chaotic maps with an invariant measure. J Stat Phys 2001;104(5–6):1013–28.
[57] Behnia S, Yahyavi M. Characterization of intermittency in hierarchy of chaotic maps with invariant measure. J Phys Soc Jpn 2012;81(12):124008–16.
[58] Cornfeld IP, Fomin SV, Sinai YG. Ergodic theory, 245. Springer Science & Business Media; 2012.
[59] Keller G. Equilibrium states in ergodic theory, 42. Cambridge university press; 1998.
[60] Behnia S, Ahadpour S, Faizi E. A novel moment approach for calculation of the perron–frobenius spectrum. Int J Theor Phys 2007;46(11):2836–42.